The Dual-Current-Loop Controlled Doubly Fed Induction Motor for EV/HEV Applications

Yu Liu, *Student Member, IEEE*, and Longya Xu, *Fellow, IEEE*

***Abstract*—With the proposed dual-current-loop control algorithm, the torque and air-gap flux of a doubly fed induction motor are controlled directly. Compared to the singly fed permanent magnet and induction motors, the torque–speed operation region for electric vehicle/hybrid electric vehicle applications is nearly doubled with the proposed dual-current-loop control algorithm for a given battery voltage. Computer simulations and experimental results are provided to verify the proposed control algorithm.**

***Index Terms*—Control of traction motor, doubly fed induction motor (DFIM), electric vehicle/hybrid electric vehicle (EV/HEV), torque–speed characteristics.**

I. Introduction

RECENTLY, electric vehicles (EVs) and hybrid electric vehicles (HEVs) have received much attention due to their high fuel efficiency and low emissions. The EV/HEV traction motors, the core components for the applications, should be designed to meet the following requirements [1]–[4]:

1) high torque density and power density;
2) wide torque–speed capability;
3) high efficiency over wide torque–speed ranges;
4) high reliability and robustness;
5) low cost in manufacturing and maintenance.

Currently, interior permanent magnet (IPM) motor and cage induction motor (IM) are the two most popular choices for EV/HEV traction motors. A rare-earth IPM motor exhibits a high torque density, wide speed–torque range, compact size, and high efficiency due to the strong magnetic field provided by the rare-earth magnets, while a cage IM has no external source for the magnetic field. To provide torque, an IM has to rely upon its rotor slip relative to the synchronous speed to generate the rotor current. As a consequence, the torque density of a cage IM is lower and size larger than that of an IPM motor. Moreover, the dual mechanical port machine and switched reluctance machine are also proposed and discussed for EV/HEV applications [5], [6].

Though often used as a variable-speed, constant-frequency generator such as in wind power, lately the doubly fed induction machine is proposed as a potential candidate for EV/HEV applications, especially for its much extended regions of both constant torque and constant power operation [7]–[11]. Both IPM motor and IM are the singly fed motors, and their system configurations for typical traction applications are shown in Fig. 1. The essential difference between a DFIM traction system and a singly fed traction system is that the DFIM system has two inverters, one for the stator windings and another for the rotor windings. In operation, both inverters are actively controlled. Fig. 2 shows the DFIM traction system with its controller and power inverters. In EV/HEV applications, there is only one battery pack and, therefore, two inverters share the same battery pack with a common dc bus voltage. The kVA ratings of the two inverters are the same and each is a half of the total system kVA rating. For optimal performance in EV/HEV traction applications, the traction motor has to be matched by a properly designed controller and several control algorithms of the DFIM have been studied [8]–[10].

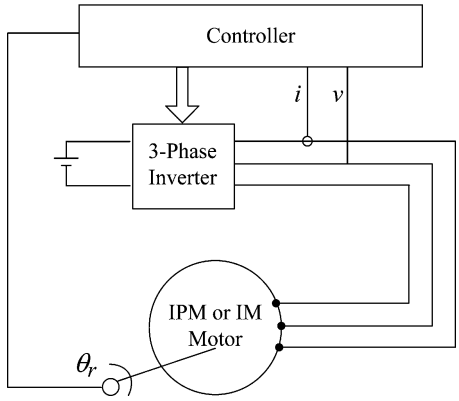

Fig. 1. Singly fed motor drive system in EV/HEV applications.

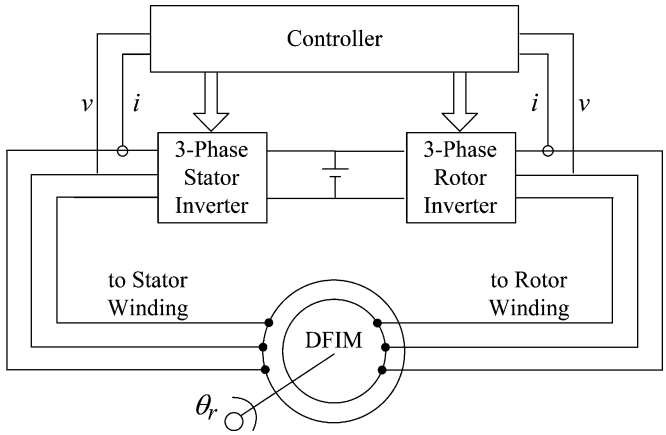

Fig. 2. DFIM drive system in EV/HEV applications.

Manuscript received April 1, 2013; revised July 10, 2013; accepted August 19, 2013. Date of publication September 9, 2013; date of current version November 20, 2013. Paper no. TEC-00195-2013.

Y. Liu and L. Xu are with the Department of Electrical and Computer Engineering, The Ohio State University, Columbus, OH 43210 USA (e-mail: liu.1010@osu.edu; xu.12@osu.edu).

Color versions of one or more of the figures in this paper are available online at http://ieeexplore.ieee.org.

Digital Object Identifier 10.1109/TEC.2013.2279853

A vector control strategy of the DFIM is proposed in [8]. In the vector control algorithm, both the stator and rotor currents are decoupled into magnetizing and torque components. However, for a DFIM, the stator and rotor magnetizing currents are coupled. For this reason, a magnetizing current decoupling controller is employed in the algorithm. In addition, a torque current decoupling controller is also designed due to the torque current of the stator, and the rotor is coupled by the stator/rotor turns ratio. Then, four current regulators are required because the magnetizing and the torque currents of the stator and the rotor are controlled independently. Four-quadrant operation experimental results are provided, but without discussion on how to determine the torque and the magnetizing current references.

In order to optimize the current references, a minimum copper loss and power distribution control strategy is proposed for the DFIM [9]. In this strategy, the motor speed is the control objective and four currents are controlled independently. Therefore, three degrees of control freedoms are available in addition to the speed control: the first one is used to manage the rotor flux, the second one to distribute power to the stator and rotor, and the last one to implement the minimum copper loss. Experimental results are provided and copper loss minimization is realized. However, the minimum copper loss strategy requires the knowledge of accurate motor parameters.

Without using the current controller, a direct torque control algorithm is introduced in [10]. In this algorithm, the torque of the DFIM is controlled through stator and rotor fluxes by using two hysteresis controllers. The idea is to maintain the stator flux and rotor flux to their nominal values so as to control the torque angle. A reduced flux model is built with the following assumptions: a) neglect the resistive effect in the windings for the considered operating frequencies and b) neglect coupling terms in the flux model. However, these two assumptions will degrade control accuracy of torque whenever the operating frequency is low and the winding resistance not negligible. Moreover, both the stator and the rotor time constants must be significantly larger than the inverter switching time, required by the direct torque control algorithm. The large time constant requirement may only be met with high power machines close to megawatt ratings. The speed tracking experimental result is provided, but issues of flux weakening region operation are not addressed in the paper. The above papers have partially demonstrated that the DFIM can be well controlled for different goals. However, these algorithms also indicate that satisfactory control algorithms are still in need with regard to using DFIM in EV/HEV applications.

In our previous research, attention is focused on efficiency comparison of a DFIM with a singly fed motor in variable speed drives and the control algorithm is treated lightly [11]. In this paper, a dual-current-loop control algorithm is proposed and investigated in detail. By controlling the torque and air-gap flux, the proposed algorithm ensures DFIM high performance in both the extended constant torque and extended constant power regions. In addition, analysis is given to confirm that the algorithm is parameter insensitive, and that neither the magnetizing current nor torque current needs to be decoupled.

Following Section I, in Section II, the torque–speed characteristics of the DFIM are reviewed to set up the necessary background for proposing the dual-current-loop algorithm. In Section III, the controller structure and principles related to the proposed dual-current-loop control algorithm are described and analyzed. In Section IV, simulations and experimental testing are conducted and results presented to verify the effectiveness of the proposed control algorithm. Finally, the paper concludes with the contribution highlights and possible future work.

II. Torque–Speed Characteristics of the DFIM

For an electric motor, its torque capability is generally constrained by the allowable current fed into the windings without excessive loss/heat. On the other hand, its speed range is constrained by the available voltage supply because the high back EMF in high speed may disable the controlling capability of the supply voltage.

Specifically, compared to an IM and IPM motors of the same size, the torque capability of a DFIM is almost the same since their current capability is about the same, only limited by the conduction losses and thermal dissipations. However, the speed range of a DFIM can be doubled because both the DFIM stator and rotor windings can be supplied with the supply voltage to handle the induced-back EMFs. The electromechanical power of the DFIM can be divided into the stator and rotor windings, equally or unequally as the controller prefers, regardless of the motor speed. The torque–speed characteristics are summarized in Fig. 3(a)–(c).

In Fig. 3(a), we assume that the DFIM is operated only as a conventional synchronous motor. In Fig. 3(b), the DFIM is operated as an IM in the subsynchronous mode and in this way, the rotor regenerates the slip power back into the voltage supply, while the stator takes power from the voltage supply. If both the stator and rotor windings are allowed to take power from the supply voltage, the base speed will be doubled and so is the constant torque region. The same argument also applies to the constant power region when the air-gap flux of the DFIM is weakened. As a result shown in Fig. 3(c), both the constant torque and constant power regions of a DFIM are doubled without a boosted dc bus voltage. The purpose of this paper is to develop an optimized control algorithm to fully explore the torque and speed capabilities of a DFIM for EV/HEV applications.

III. Proposed Dual-Current-Loop Control Algorithm

The dynamic equations of a DFIM can be written in (1) through (10) and are utilized to develop the DFIM control algorithm:

$$v_{ds} = R_s i_{ds} + \frac{d\lambda_{ds}}{dt} - \omega_s \lambda_{qs} \tag{1}$$

$$v_{qs} = R_s i_{qs} + \frac{d\lambda_{qs}}{dt} + \omega_s \lambda_{ds} \tag{2}$$

$$\lambda_{ds} = L_s i_{ds} + L_m i_{dr} \tag{3}$$

$$\lambda_{qs} = L_s i_{qs} + L_m i_{qr} \tag{4}$$

$$v_{dr} = R_r i_{dr} + \frac{d\lambda_{dr}}{dt} - \omega_r \lambda_{qr} \tag{5}$$

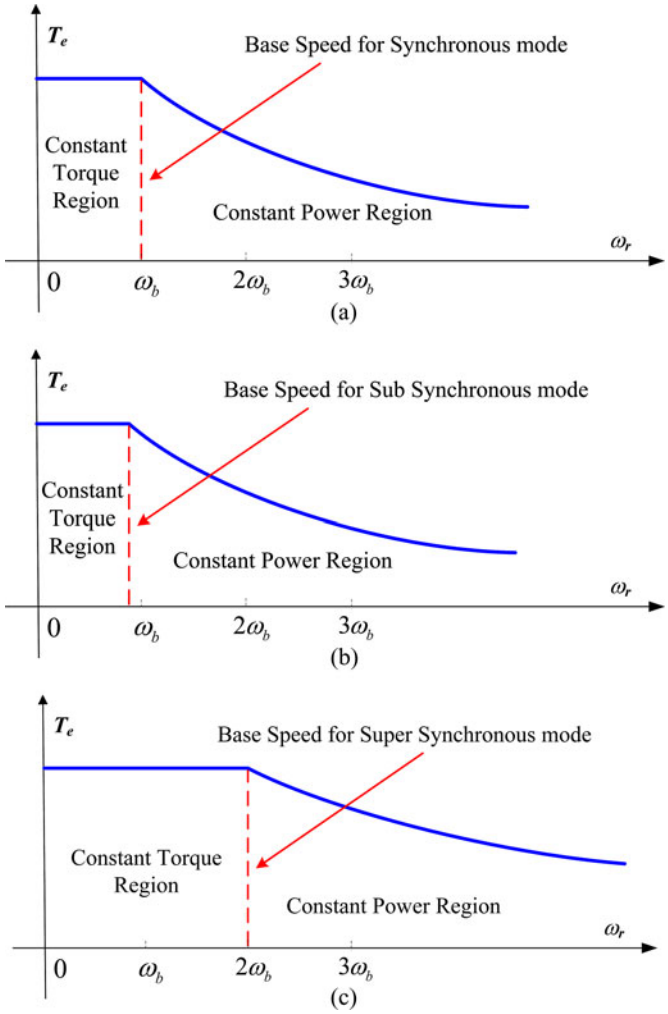

Fig. 3. Torque–speed characteristics of the DFIM. (a) Synchronous mode. (b) Subsynchronous mode. (c) Supersynchronous mode.

$$v_{qr} = R_r i_{qr} + \frac{d\lambda_{qr}}{dt} + \omega_r \lambda_{dr} \tag{6}$$

$$\lambda_{dr} = L_r i_{dr} + L_m i_{ds} \tag{7}$$

$$\lambda_{qr} = L_r i_{qr} + L_m i_{qs} \tag{8}$$

$$T_e = 1.5p\frac{L_m}{L_s}\left(\lambda_{qs} i_{dr} - \lambda_{ds} i_{qr}\right) \tag{9}$$

$$\omega_{mr} = \frac{1}{p}\omega_{er} = \frac{1}{p}\left(\omega_s + \omega_r\right). \tag{10}$$

The subscripts "s" and "r" refer to the variables associated with the stator and rotor windings, respectively. v_s and v_r are the stator and rotor voltages; i_s and i_r are the stator and rotor currents; R_s and R_r are the stator and rotor resistance; L_m, L_s, and L_r are the magnetizing, stator, and rotor inductances, respectively; λ_s and λ_r are the stator and rotor flux linkages; ω_s is the stator winding electrical angular velocity and ω_r is the rotor winding electrical angular velocity; ω_{mr} is the rotor mechanical angular velocity and ω_{er} is the rotor electrical angular velocity in radius per second; and p is the pole pair number. Note that (10) works when the stator phase sequence is different from the rotor phase sequence, as the stator phase sequence is clockwise and the rotor phase sequence anticlockwise.

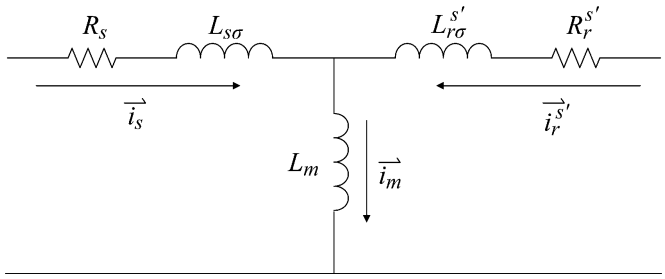

Fig. 4. DFIM equivalent circuit in the vector notation.

A. Principles of the DFIM Dual-Current-Loop Algorithm

To illustrate the principles of the control algorithm, it is conveniently to describe the DFIM dynamics in the vector format. As stated in the previous section, T_e is the electromagnetic torque that can be rewritten in the vector form as

$$T_e = 1.5pL_m(\vec{i}_s \times \vec{i}_r^{s\prime}) \tag{11}$$

$$T_e = 1.5pL_m i_s i_r^{s\prime} \sin\delta \tag{12}$$

where $\vec{i}_r^{s\prime}$ is the rotor current vector referred to the stator side, in terms of the magnitude and angle transformation. The magnitude transformation is decided by the stator/rotor turns ratio (n_s/n_r) and the angle transformation is decided by the rotor electrical angle θ_{er}. In the vector format, the relationships among the various current vectors are as follows:

$$\vec{i}_s = i_s \angle \theta_s \tag{13}$$

$$\vec{i}_r = i_r \angle \theta_r \tag{14}$$

$$i_r^{s\prime} = i_r \times \left(\frac{n_r}{n_s}\right) \tag{15}$$

$$\vec{i}_r^{s\prime} = i_r^{s\prime} \angle \theta_r^{s\prime} = i_r^{s\prime} \angle (\theta_r + \theta_{er}) \tag{16}$$

$$\delta = \theta_s - \theta_r^{s\prime} = \theta_s - \theta_r - \theta_{er} \tag{17}$$

where θ_s is the stator current angle and θ_r is the rotor current angle; $\theta_r^{s\prime}$ stands for the angle of current vector $\vec{i}_r^{s\prime}$; the current phase shift angle δ represents the angular difference between $\vec{i}_s$ and $\vec{i}_r^{s\prime}$.

In terms of the vector notation, the DFIM equivalent circuit has been depicted in Fig. 4.

The relationship among the stator current $\vec{i}_s$, rotor current $\vec{i}_r^{s\prime}$, and magnetizing current $\vec{i}_m$ can be simply described by the vector diagram as shown in Fig. 5.

As illustrated by the vector diagram, the magnetizing current is the sum of the stator and rotor current vectors that can be written as

$$\vec{i}_m = + \vec{i}_s + \vec{i}_r^{s\prime} \tag{18}$$

with its magnitude given by

$$i_m = \sqrt{i_s^2 + i_r^{s\prime 2} + 2i_s i_r^{s\prime}\cos\delta}. \tag{19}$$

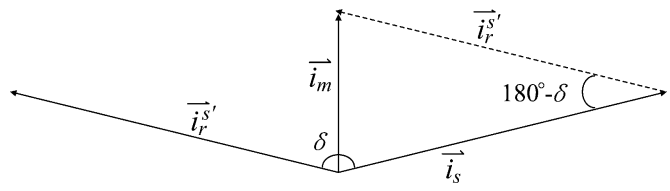

Fig. 5. Stator and rotor current vector diagram.

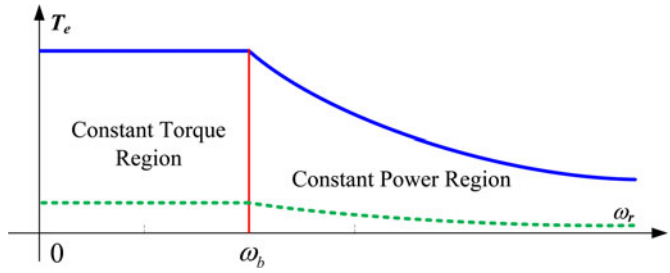

Fig. 6. Constant torque and constant power region of the DFIM.

The air-gap flux linkage can be obtained by

$$\lambda_m = L_m i_m = L_m \sqrt{i_s^2 + i_r^{s\prime 2} + 2 i_s i_r^{s\prime} \cos\delta}. \quad (20)$$

Note that the vector expressions of the electromagnetic torque and air-gap flux in (12) and (20) form the kernel for the proposed dual-current-loop control algorithm. It is noted that there are three degrees of control freedoms as evidenced by (12) and (20): the amplitudes of $\vec{i}_s$ and of $\vec{i}_r^{s\prime}$, and the phase angle δ between the two current vectors. Controlling the torque and air-gap flux only takes two degrees of freedoms. In our proposed control algorithm, the third control freedom is proposed for maximum torque per ampere purpose. For the rotor current control, the control objective will be identical to that of the stator and, therefore, no additional control freedoms will be needed for the rotor, which can be expressed by

$$i_s = i_r^{s\prime} = i_{eq}. \quad (21)$$

Then, (12) and (19) become

$$T_e = 1.5 p L_m i_{eq}^2 \sin\delta \quad (22)$$

$$i_m = \sqrt{2 i_{eq}^2 + 2 i_{eq}^2 \cos\delta}. \quad (23)$$

It is clearly shown by (22) that, for a given i_{eq}, the maximum torque can be achieved whenever δ is equal to 90°. In (23), the magnetizing current i_m can be regulated by controlling i_{eq} and δ. So, there is no need to split the magnetizing current into additional the stator and rotor components. For a given i_{eq}, as δ increases from 0° to 180°, the magnetizing current i_m decreases from $2i_{eq}$ to 0 accordingly.

B. Implementation of the Dual-Current-Loop Algorithm

The proposed control algorithm is designed and implemented for variable speed operation in EV/HEV applications. The torque–speed characteristics of a DFIM are shown in Fig. 6. The implementation of the proposed dual-current-loop control algorithm is shown by the controller block diagram in Fig. 7. The dual-current-loop algorithm can generate the right values of i_{eq} and δ for each operating point inside both the constant torque and constant power regions.

In the constant torque region, the primary goal is to provide sufficient torque and fast dynamic response. To meet this goal, the proposed control algorithm keeps the maximum allowable air-gap flux without core saturation. Then, the torque demand is satisfied by the dual current close loops.

In the constant power region, the top priority is to control the flux weakening level because the DFIM will have stability problems when it works without the flux weakening control. Flux weakening controls are also required for IPM and IM working beyond base speed, a negative magnetizing current is needed to demagnetize PMs in the IPM flux weakening control, and a reduced magnetizing current is needed in the IM flux weakening control [12]–[16]. Therefore, the flux weakening control is desired and included in the proposed algorithm. The air-gap flux is controlled directly by the magnetizing current, which turns the air-gap flux control into the magnetizing current control. In Fig. 7, the magnetizing current reference is obtained from a flux controller which can be implemented by different methods. An open loop algorithm is used in this paper which sets the magnetizing current reference inversely proportional to the speed in the constant power region. By using this algorithm, the magnetizing current decreases as speed increases when the DFIM works beyond base speed.

Another function of the flux weakening control is to realize the full utilization of the maximum inverter voltage. This is because if the inverter voltage is not fully utilized, then the DFIM will need more current than necessary, resulting in high conduction losses in both the motor and inverter. The air-gap flux weakening control of the DFIM is achieved by reducing the magnetizing current through controlling the angle difference δ between the stator and rotor current vectors $\vec{i}_s$ and $\vec{i}_r^{s\prime}$. Based on the magnetizing current, stator current, and rotor current, the current phase shift angle δ can be calculated by the following equation:

$$\delta = \cos^{-1}\left(\frac{i_m^2 - i_s^2 - i_r^{s\prime 2}}{2 i_s i_r^{s\prime}}\right). \quad (24)$$

Note that in Fig. 6, there is a region below the green dashed line where i_{eq} could be so small that it could result in a very small magnetizing current $\vec{i}_m$. In such a situation, the air-gap flux λ_m will become much smaller than the allowable and desirable levels in the constant torque region and constant power region. To avoid the too small flux levels as previously mentioned, we can let δ be equal to 90° so that we can achieve the objectives of both the maximum torque per ampere objective and reasonable air-gap flux level.

The implementation of the proposed dual current control of the DFIM is based on the above principle discussion. The essential and ultimate goal is to control the DFIM to the desired flux level and torque production. The directly controlled system variables, based on (12) and (19), will be the three variables of

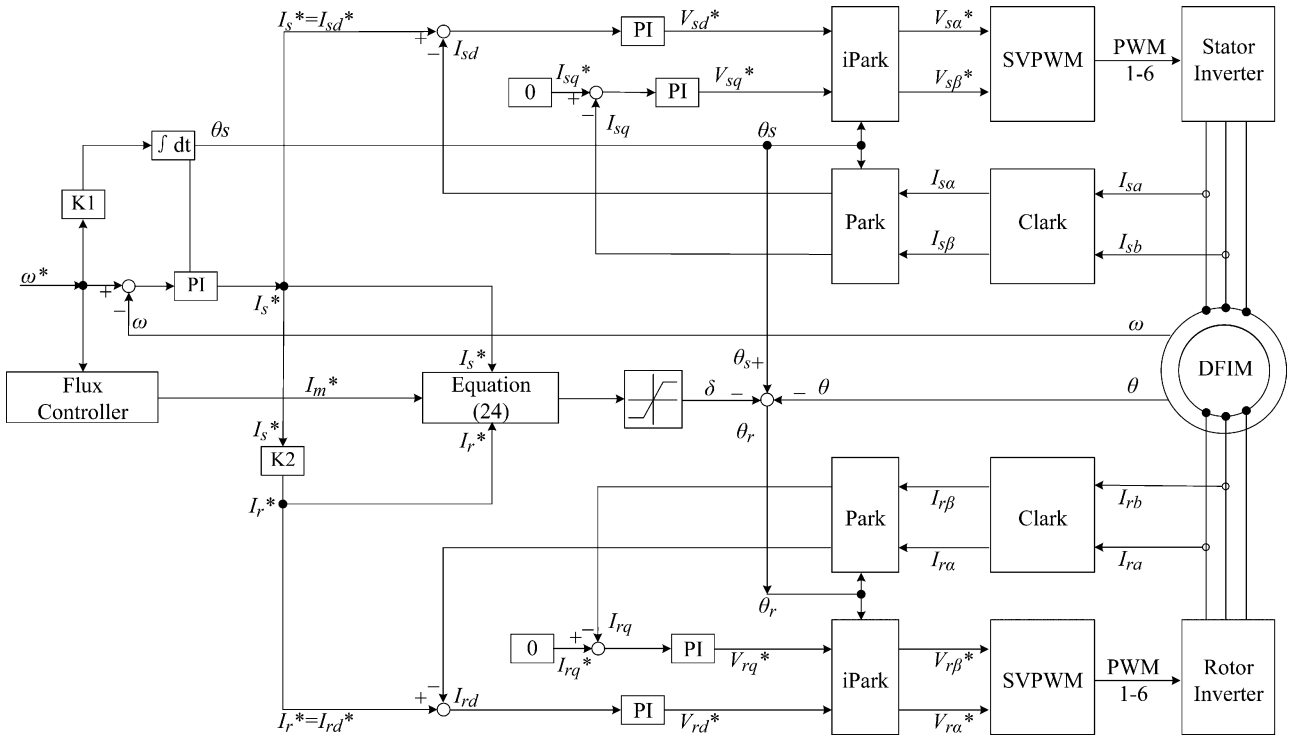

Fig. 7. Block diagram of the control algorithm for the DFIM drive system.

the currents, that is, the stator and rotor currents, i_s and i_r, and their angle difference δ. As illustrated in Fig. 7, all the three variables can be regulated through the current closed loop control. The current closed loop control based on the PI regulator can be designed by frequency response, genetic algorithm, poles placement, complex vector, real-time gain tuning, and internal model control method [17]–[21]. The current regulator design in this paper is made by trial and error with consideration of transient response, overshoot, oscillation, and saturation. For all current regulators, the proportional gain K_p is 2.75 Ω and integral gain K_i is 0.0045 Ω/s. In the controller block diagram, the torque reference is generated automatically by the speed PI regulator. The air-gap flux reference is set to the rated flux level when the DFIM works in the constant torque region and inversely proportional to the speed in the constant power region. For a given air-gap flux, the current phase shift angle δ is obtained through (24). If δ is less than 90°, we will set δ to 90° for the maximum torque per ampere purpose.

In the control block diagram, $K1$ is the gain of speed reference used to determine the stator winding electrical angular velocity and $K2$ is the ratio of the rotor current to stator current. In order to make the stator and rotor windings work with the same frequency, $K1$ is set to 0.5 in the implementation. For the maximum torque per ampere control, $K2$ is set to 1 as indicated. However, both $K1$ and $K2$ are adjustable if desired for any special purposes. Note that the *d–q* decoupling notations used in Fig. 7 have no relevance to the real magnetizing and torque components. The *d–q* decoupling loops in the control block diagram are only used to control the stator and rotor current vectors.

TABLE I
RATING AND PARAMETERS OF DFIM

Nominal power	1 hp
Nominal stator line-to-line voltage	230 V
Nominal rotor line-to-line voltage	90 V
Nominal stator phase current	3.6 A
Nominal rotor phase current	6.0 A
Number of pole pairs	2
Base speed	1200 rpm
Stator/rotor resistance	2.85/1.25 Ω
Stator/rotor leakage inductance	22.4/12.8 mH
Mutual inductance	164.6 mH

IV. SIMULATION AND EXPERIMENTAL VERIFICATION

Computer simulation and experimental testing are conducted to verify the dual-current-loop control algorithm and results are summarized in this section. The specifications and parameters of the DFIM in simulation and testing are listed in Table I.

A. Simulation Investigation and Results

A computer model of the DFIM system with the proposed dual-current-loop control algorithm as shown in Fig. 7 has been developed in the PSIM simulator. In simulation, the DFIM system is investigated to track a speed command in four-quadrant operation from 1800 to −1800 r/min within 1.2 s. The reason to investigate the DFIM in the speed range of ±1800 r/min is

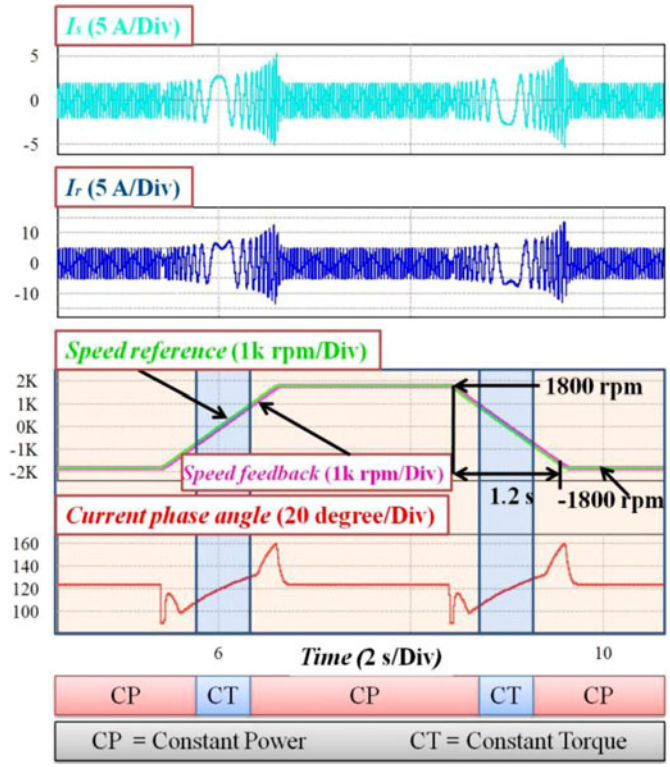

Fig. 8. Simulation results of the DFIM in four-quadrant operation.

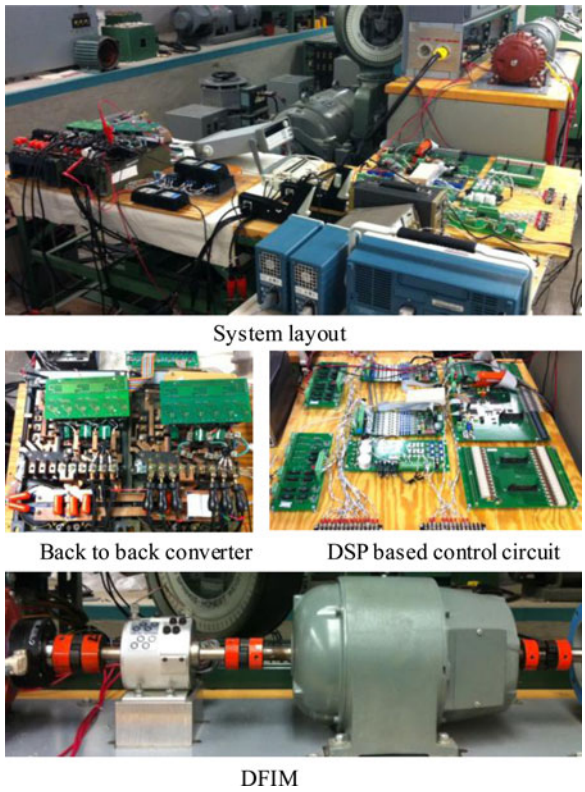

Fig. 9. DFIM experimental system.

to let the DFIM experience both the motoring and generating modes in both directions and covering speeds below and above the base speed of 1200 r/min. The speed tracking performance is shown in Fig. 8. From the top to bottom are the traces of the stator current, rotor current, speed command and simulated actual speed, and the current angle between the stator and rotor current vectors. As the results indicate, we have controlled the stator and rotor currents and frequencies (power) equally over the entire speed range through the proposed dual-current-loop algorithm. It is also notable that the current magnitudes of the stator and rotor currents are different. This is because the turn numbers of the stator and rotor windings are different. In addition, the phase angle between the stator and rotor current vectors is always controlled as a variable to optimize the torque production and magnetizing current for either constant torque or constant power mode.

As expected, with the dual-current-loop control algorithm, the DFIM system works well in both the constant torque and constant power regions. The phase angle δ is adjusted by the algorithm automatically and satisfactory torque and speed performance is achieved. It should be pointed out that for the speed range covered in simulation, the applied voltage to the DFIM is only half of the voltage needed for an equivalent singly fed IPM and IM machines.

B. Experimental Testing and Measured Results

To further verify the effectiveness of the proposed control algorithm, experimental testing is conducted on an actual DFIM system with the same specifications and parameters as those specified in computer simulation. Fig. 9 shows a photo of the lab setup of the DFIM system, including the DFIM, the back-to-back converter consisting of two identical inverters, and the DSP-based control hardware and software.

Note that in the experiment, the dc bus voltage of the inverters is 200 V, only a half value of dc bus voltage for the same DFIM system to run in the speed range of ± 1800 r/min if it were singly fed. The experimental testing results are shown in Fig. 10.

In the testing, the DFIM is commanded to track a speed reference similar to that used in the simulation. The speed reversal from $+1800$ to -1800 r/min is also commanded to accomplish within 1.2 s.

The recorded results by a digital scope are explained here. Trace 1 is the rotor current, trace 2 the stator phase current, trace 3 the actual speed, and trace 4 the speed command. The phase angle between the stator and rotor current vectors phase angle cannot be recorded due to the equipment limit. As shown by the actually recorded traces, the DFIM speed tracking performance is achieved and satisfactory.

Compared to the simulation results, the amplitudes of the actual currents are slightly different due to the differences in frication and inertia between the simulation model and the real system. However, both results show a very good dynamic speed response and the results from simulation and actual experimental testing are in good agreement in general. It is evident that with proposed dual-current-control algorithm, the DFIM system is well controlled both in the motoring and generating modes, covering both the constant torque and constant power regions in either rotating direction.

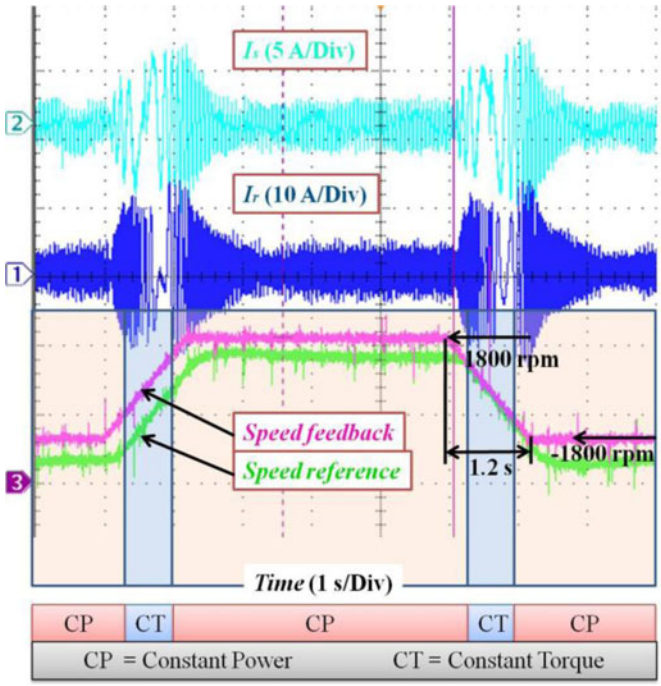

Fig. 10. Experimental results of the DFIM in four-quadrant operation.

V. Conclusion

With an original idea of the dual-current-loop algorithm, this paper contributes to the control of DFIMs for EV/HEV applications. The concept and features of the proposed dual-current-loop control algorithm are described in detail.

By analytical investigation, computer simulation, and experimental testing, the merits of the proposed dual-current-control algorithm are revealed and fully verified. The advantages of applying the proposed control algorithm to a DFIM include the following.

1) In both the constant power and constant torque regions, the torque and air-gap flux of the DFIM are directly controlled by the two current vectors, providing a stable and accurate powertrain solution to EV/HEV application.
2) The amplitudes of the stator and rotor current vectors and the phase angle between them provide three degrees of control freedoms. In additional to the torque and flux control, one control freedom can be used for maximum torque per ampere or efficiency control for the DFIM.
3) When the algorithm is applied, only half of a dc bus voltage is required to achieve the full torque–speed range, or doubled torque–speed range if a rated dc bus voltage is used, compared to an equivalent singly fed machine. This is valuable and an attractive feature to EV/HEV applications.
4) The DFIM system with the proposed algorithm has less dependence on motor parameters than the other types of control algorithms for singly fed motor or DFIM. In the proposed algorithms, magnetizing inductance L_m is the only needed parameter.

Different from the conventional DFIM control with only a rotor side control loop, the dual loop control of both the stator and rotor sides of a DFIM is an interesting and not well-explored area. More research activities are planned and currently in progress using the dual current loop and other algorithms. New results from the planned research including motion sensorless control and brushless DFIM will be reported in our future papers.

References

[1] Z. Q. Zhu and D. Howe, "Electrical machines and drives for electric, hybrid, and fuel cell vehicles," *Proc. IEEE*, vol. 95, no. 4, pp. 746–765, Apr. 2007.
[2] K. T. Chau, C. C. Chan, and C. Liu, "Overview of permanent-magnet brushless drives for electric and hybrid electric vehicles," *IEEE Trans. Ind. Electron.*, vol. 55, no. 6, pp. 2246–2257, Jun. 2008.
[3] G. Pellegrino, A. Vagati, B. Boazzo, and P. Guglielmi, "Comparison of induction and PM synchronous motor drives for EV application including design examples," *IEEE Trans. Ind. Appl.*, vol. 48, no. 6, pp. 2322–2332, Nov./Dec. 2012.
[4] M. Zeraoulia, M. E. H. Benbouzid, and D. Diallo, "Electric motor drive selection issues for HEV propulsion systems: A comparative study," *IEEE Trans. Veh. Technol.*, vol. 55, no. 6, pp. 1756–1764, Nov. 2006.
[5] L. Xu, Y. Zhang, and X. Wen, "Multioperational modes and control strategies of dual-mechanical-port machine for hybrid electrical vehicles," *IEEE Trans. Ind. Appl.*, vol. 45, no. 2, pp. 747–755, Mar./Apr. 2009.
[6] K. M. Rahman, B. Fahimi, G. Suresh, A. V. Rajarathnam, and M. Ehsani, "Advantages of switched reluctance motor applications to EV and HEV: Design and control issues," *IEEE Trans. Ind. Appl.*, vol. 36, no. 1, pp. 111–121, Jan./Feb. 2000.
[7] H. S. Song, K. Nam, H. R. Choi, and H. G. Kim, "A new topology and control scheme for 4WD HEV using a DFIM with a reduced size converter-inverter," in *Proc. IEEE 40th Ind. Appl. Conf.*, 2005, vol. 4, pp. 2880–2886.
[8] Y. Kawabata, E. Ejiogu, and T. Kawabata, "Vector-Controlled double-inverter-fed wound-rotor induction motor suitable for high-power drives," *IEEE Trans. Ind. Appl.*, vol. 35, no. 5, pp. 1058–1066, Sep./Oct. 1999.
[9] K. Chen, P. Delarue, A. Bouscayrol, P. Vidal, and M. Pietrzak-David, "Minimum copper loss and power distribution control strategies of double-inverter-fed wound-rotor induction machines using energetic macroscopic representation," *IEEE Trans. Energy Convers.*, vol. 25, no. 3, pp. 642–651, Sep. 2010.
[10] F. Bonnet, P. Vidal, and M. Pietrzak-David, "Dual direct torque control of doubly fed induction machine," *IEEE Trans. Power Electron.*, vol. 54, no. 5, pp. 2482–2490, Oct. 2007.
[11] L. Xu and Y. Liu, "Comparison study of singly-fed electric machine with doubly-fed machine for EV/HEV applications," in *Proc. IEEE Int. Conf. Elect. Mach. Syst.*, 2011, pp. 1–5.
[12] T. M. Jahns, "Flux-Weakening regime operation of an interior permanent-magnet synchronous motor drive," *IEEE Trans. Ind. Appl.*, vol. IA-23, no. 4, pp. 681–689, Jul./Aug. 1987.
[13] L. Xu, Y. Zhang, and M. K. Güven, "A new method to optimize q-axis voltage for deep flux weakening control of IPM machines based on single current regulator," in *Proc. IEEE Int. Conf. Elect. Mach. Syst.*, 2008, pp. 2750–2754.
[14] S. Kim and S. Sul, "Maximum torque control of an induction machine in the field weakening region," *IEEE Trans. Ind. Appl.*, vol. 31, no. 4, pp. 787–794, Jul./Aug. 1995.
[15] J. Seok and S. Sul, "Optimal flux selection of an induction machine for maximum torque operation in flux-weakening region," *IEEE Trans. Power Electron.*, vol. 14, no. 4, pp. 700–708, Jul. 1999.
[16] R. J. Kerkman, T. M. Rowan, and D. Leggate, "Indirect field-oriented control of an induction motor in the field-weakening region," *IEEE Trans. Ind. Appl.*, vol. 28, no. 4, pp. 850–857, Jul./Aug. 1992.
[17] G. W. Chang, G. Espinosa-Perez, E. Mendes, and R. Ortega, "Tuning rules for the PI gains of field-oriented controllers of induction motors," *IEEE Trans. Ind. Appl.*, vol. 47, no. 3, pp. 592–602, Jun. 2000.
[18] J. P. A. Vieira, M. N. A. Nunes, and U. H. Bezerra, "Design of optimal PI controllers for doubly fed induction generators in wind turbines using genetic algorithm," in *Proc. IEEE Power Energy Soc. General Meeting*, 2008, pp. 1–7.
[19] F. Briz, M. W. Degner, and R. D. Lorenz, "Dynamic analysis of current regulators for AC motors using complex vectors," *IEEE Trans. Ind. Appl.*, vol. 35, no. 6, pp. 1424–1432, Nov./Dec. 1999.

[20] M. Tursini, F. Parasiliti, and D. Zhang, "Real-time gain tuning of PI controllers for high-performance PMSM drives," *IEEE Trans. Ind. Appl.*, vol. 38, no. 4, pp. 1018–1026, Jul./Aug. 2002.

[21] L. Harnefors and H. P Nee, "Model-based current control of AC machines using the internal model control method," *IEEE Trans. Ind. Appl.*, vol. 34, no. 1, pp. 133–141, Jan./Feb. 1998.

Yu Liu (S'13) received the B.S. degree in electrical engineering from Southeast University, Nanjing, China, in 2008. He is currently working toward the Ph.D. degree in electrical engineering at The Ohio State University, Columbus, OH, USA.

His research interests include variable-speed drive control, power electronics for electric vehicles, and electric machine design.

Longya Xu (S'89–M'90–SM'93–F'04) received the M.S. and Ph.D. degrees from the University of Wisconsin, Madison, in 1986 and 1990 both in electrical engineering. He joined the Department of Electrical Engineering at The Ohio State University in 1990, where he is presently a Professor. He has served as a consultant to many industry companies including Raytheon Co., Boeing, Honeywell, GE Aviation, US Wind Power Co., General Motor, Ford and Unique Mobility Inc. for various industrial concerns. Dr. Xu is the director of the newly established Center of High Performance Power Electronics (CHPPE) at The Ohio State University, supported by The Ohio Third Frontier Program.

Dr. Xu received the 1990 First Prize Paper Award in the Industry Drive Committee, IEEE/IAS. In 1991, he won a Research Initiation Award from National Science Foundation for Wind Power Generation. He is also a recipient of 1995, 1999, and 2004 Lumley Research Award for his outstanding research accomplishments from College of Engineering, The Ohio State University. He research and teaching interests include dynamics and optimized design of special electrical machines and power converters for variable speed systems, application of advanced control theory and digital signal processor for motion control and distributed power systems in super-high speed operation. In the 20 years, he has conducted many research projects on electrical and hybrid electrical vehicles and variable speed constant frequency wind power generation systems. He has served as the chairman of Electric Machine Committee of IEEE/IAS and an Associate Editor of IEEE Transactions on Power Electronics in the past several years. He currently is serving as a member-at-large on IEEE/IAS Executive Board.